J. Fluid Mech. (1989), *vol.* 198, *pp.* 231–254
Printed in Great Britain

Selective withdrawal from a viscous two-layer system

By JOHN R. LISTER

Research School of Earth Sciences, Australian National University,
PO Box 4, Canberra 2601, A.C.T., Australia

(Received 28 January 1988 and in revised form 11 June 1988)

When fluid is withdrawn from a body of stratified fluid the surfaces of constant density are deformed towards the region of withdrawal. The equations describing the flow caused by withdrawal through a point sink in a two-layer unbounded system in which viscous forces dominate are formulated using the boundary-integral representation of Stokes flow. It is shown by dimensional and analytic arguments that surface tension between the layers is a necessary condition for the stability of an interfacial equilibrium in which only one fluid is withdrawn. The critical flow rate above which both fluids are withdrawn is determined numerically as a function of the capillary number. When the flow is supercritical a small adaptation of the numerical scheme allows the proportion of fluid withdrawn from each layer to be found. The various analyses and conclusions further our understanding of the physical processes that determine the compositional output of volcanic eruptions that tap an underlying stratified reservoir of magma.

1. Introduction

It is very common for the density of naturally occurring bodies of fluid to vary with height. A 'selective withdrawal' problem poses the following questions:

(i) If a sink is introduced into such a stratified environment, will fluid be selectively withdrawn from a horizontal fluid layer containing the sink, or will the flow deform the density surfaces so that a mixture of fluids of different densities is extracted?

(ii) If a mixture of fluids is extracted what proportion of the mixture is withdrawn from each level?

A range of such problems, with discontinuous and continuous density distributions, in two-dimensional and axisymmetric geometries, has been studied in the inertial parameter regime. A review of this work may be found in Imberger (1980). The particular cases of two-dimensional flow that is either inviscid and irrotational or in an isotropic porous medium have been investigated by conformal-mapping techniques (Craya 1949; Bear & Dagan 1964; Tuck & Vanden-Broeck 1984). The problems described so far are appropriate to fields such as the effects on water purity of outflow from reservoirs and aquifers. In this paper we discuss the much less considered regime of viscous withdrawal from a layered system, which has applications, in particular, to the field of igneous geology.

Compositional zonation in deposits from volcanic eruptions has been used to infer the existence of stratification in the contents of the magma chamber feeding the eruption (see review in Hildreth 1981). Recent models of the thermal and chemical evolution of magma chambers have shown that fractional crystallization and double-

diffusive effects can cause this stratification (Sparks, Huppert & Turner 1984; Huppert & Sparks 1984). The consequent interest in the structure of the stratification has prompted investigations into the selectivity of the withdrawal of magma from the chamber during the course of a volcanic eruption (Spera 1984; Blake & Ivey 1986) and the effect on the mineral composition of the eruption products (Koyaguchi 1985; Freundt & Tait 1986; Spera *et al.* 1986). The numerical simulations of Spera (1984), however, did not include the effects of density stratification. Experimental work, described in Blake & Ivey (1986), did not investigate the effects of surface tension. We present both analytic and numerical results which show that both buoyancy and surface tension play an important role in an accurate description of viscous selective withdrawal.

Motivated by the geological application, we consider axisymmetric withdrawal from a point sink located, for simplicity, within the upper of two semi-infinite layers of viscous fluid with different densities and equal viscosities. The extension to the case of unequal viscosities is described briefly in Appendix B. We note that the flow in a magma chamber is often at low Reynolds number due to the extremely large viscosity of many melts. Inertial forces are assumed, therefore, to be negligible everywhere, so that the fluids are in Stokes flow. If the dimensions of the sink are small in comparison with the distance between the interface and the sink then the breakdown of this assumption in the immediate neighbourhood of the sink will not affect the analysis. In §2 we derive an integral equation describing the interfacial motion, and we use dimensional analysis to show that the system is characterized by the dimensionless flow rate and the ratio of surface tension to buoyancy forces. In §3 we present arguments showing that surface tension is necessary for the stability of an equilibrium position of the interface and in Appendix A we derive an analytic solution for such an equilibrium in the limit of small interfacial deformation.

The boundary-integral representation of Stokes flow has been found a suitable basis for numerical solution of creeping-flow problems (e.g. Youngren & Acrivos 1975; Rallison & Acrivos 1978; Lee & Leal 1982; Geller, Lee & Leal 1986). In §4 we describe a computational scheme for the integration of the boundary-integral equation of motion given in §2. Numerical simulations confirm the theoretical predictions derived in §3 and in Appendix A. Results for the critical flow rate beyond which withdrawal of both layers must occur are given in §5. For conditions in which both layers are withdrawn, the proportion extracted from each layer is calculated numerically as a function of flow rate in §6. Our conclusions are presented in §7.

2. Formulation of the problem

Consider a semi-infinite layer of fluid of density ρ_+ overlying another such layer of density ρ_- ($>\rho_+$). (See figure 1 for a definition sketch.) Let the fluids be immiscible and, for simplicity, of equal viscosity μ. In cylindrical polar coordinates (r, θ, z), let the interface between the two fluids be disturbed from its initial position at $z = 0$ to $z = f(r, t)$ by the introduction of a sink of strength q on the axis of symmetry at $z = h$. This deformation is resisted by the effects of gravity and interfacial tension.

We assume that inertial forces are negligible. Thus the equations of fluid motion reduce to

$$\nabla \cdot \boldsymbol{u} = 0, \quad \mu \nabla^2 \boldsymbol{u} = \nabla P_\pm, \tag{2.1a, b}$$

where the modified pressures $P_\pm$ are given by

$$P_\pm = p + \rho_\pm g z, \tag{2.2}$$

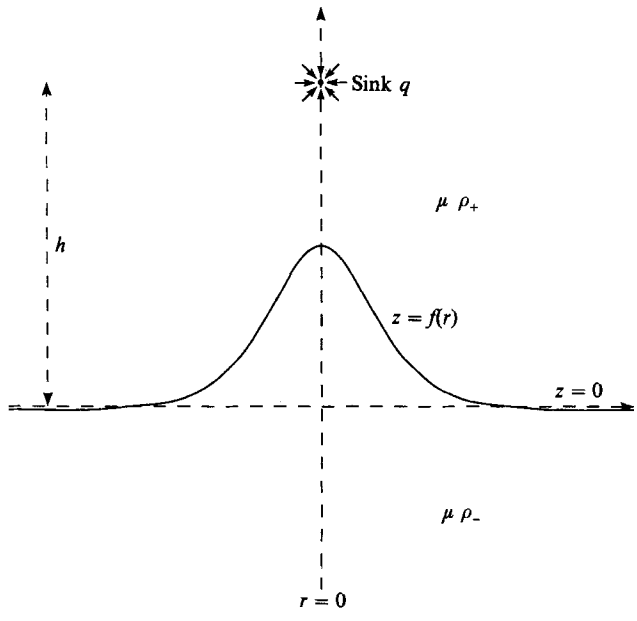

FIGURE 1. Definition sketch. A sink of strength q is introduced at a distance h above an interface between two fluids initially at $z = 0$. The interface deforms to $z = f(r, t)$.

p is the dynamic pressure, g is the acceleration due to gravity and the appropriate value for ρ is taken in $z > f$ and $z < f$. The flow is the linear superposition of sink flow

$$\boldsymbol{u}^{\mathrm{s}} = -\frac{q}{4\pi}\frac{\boldsymbol{R}}{R^3}, \quad P^{\mathrm{s}}_{\pm} = 0, \tag{2.3}$$

where $\boldsymbol{R}$ is the displacement from the sink, and the flow $\boldsymbol{u}^{\mathrm{d}}$ driven by the buoyancy and interfacial forces arising from the deformation of the interface. We express the velocity $\boldsymbol{u}^{\mathrm{d}}$ using the general identities for Stokes flow given by Ladyzhenskaya (1963):

$$-\frac{3}{4\pi}\int_{\partial V}\frac{r_i r_j r_k}{|\boldsymbol{r}|^5}u_j n_k \,\mathrm{d}A(\boldsymbol{y}) + \frac{1}{8\pi\mu}\int_{\partial V}\left(\frac{\delta_{ij}}{|\boldsymbol{r}|}+\frac{r_i r_j}{|\boldsymbol{r}|^3}\right)\sigma_{jk} n_k \,\mathrm{d}A(\boldsymbol{y}) = \begin{cases} u_i(\boldsymbol{x}) & \boldsymbol{x}\in V \quad (2.4a) \\ \tfrac{1}{2}u_i(\boldsymbol{x}) & \boldsymbol{x}\in \partial V \quad (2.4b) \\ 0 & \boldsymbol{x}\in V^*, \quad (2.4c) \end{cases}$$

where $\boldsymbol{u}$ is a Stokes flow with stress tensor $\boldsymbol{\sigma}$ in domain V with boundary ∂V, outward normal $\boldsymbol{n}$ and complementary space V^* and where $\boldsymbol{r} = \boldsymbol{x} - \boldsymbol{y}$. We apply (2.4*b*) to the Stokes flow $\boldsymbol{u}^{\mathrm{d}}$ in each of the domains $z > f$ and $z < f$ for a point $\boldsymbol{x}$ lying on the interface, and add the results. The contributions from the hemispheres at infinity are zero since $\boldsymbol{u}^{\mathrm{d}}$ is a locally driven flow. The two integrals involving $\boldsymbol{u}(\boldsymbol{y})$ cancel as a

result of the continuity of velocity across the interface and the difference in sign of the outward normal to the two fluid volumes. Thus

$$u_i^{\mathrm{d}}(\boldsymbol{x}) = \frac{1}{8\pi\mu}\int_{z=f(r)} \left(\frac{\delta_{ij}}{|\boldsymbol{r}|}+\frac{r_i r_j}{|\boldsymbol{r}|^3}\right) F_j \,\mathrm{d}A(\boldsymbol{y}), \tag{2.5}$$

where F_i is the jump in $\sigma_{ij} n_j$ across the interface. Here

$$\sigma_{ij} = -(p+\rho_{\pm} gz)\,\delta_{ij} + 2\mu e_{ij} \tag{2.6}$$

since we are using the modified pressure gradients in (2.1). The jump in this modified stress tensor is composed of the jump in the true stress tensor, $-p\delta_{ij}+2\mu e_{ij}$, due to the interfacial tension and the jump in the modified pressure due to the density discontinuity. Hence

$$\boldsymbol{F} = ((\rho_- - \rho_+) gf - \gamma\kappa)\,\boldsymbol{n} = F\boldsymbol{n}, \tag{2.7}$$

say, where γ is the coefficient of interfacial tension, and the normal $\boldsymbol{n}$ and curvature κ of the surface are given by

$$\boldsymbol{n} = \frac{(f', 0, -1)}{(1+f'^2)^{\frac{1}{2}}} \tag{2.8}$$

and

$$\kappa = \nabla\cdot\boldsymbol{n} = \frac{f''+(1+f'^2)f'/r}{(1+f'^2)^{\frac{3}{2}}}, \tag{2.9}$$

where f' and f'' denote $\mathrm{d}f/\mathrm{d}r$ and $\mathrm{d}^2f/\mathrm{d}r^2$ respectively.

The azimuthal integral in (2.5) may be evaluated using the axisymmetry of the problem. We find that $\boldsymbol{u}^{\mathrm{d}}$ has no swirl and its remaining components are given by

$$\begin{pmatrix} u_r^{\mathrm{d}}(r) \\ u_z^{\mathrm{d}}(r) \end{pmatrix} = \frac{1}{8\pi\mu}\int_0^\infty \begin{pmatrix} \mathscr{K}_{rr} & \mathscr{K}_{rz} \\ \mathscr{K}_{zr} & \mathscr{K}_{zz} \end{pmatrix} \begin{pmatrix} f'(r') \\ -1 \end{pmatrix} F(r')\, r'\,\mathrm{d}r', \tag{2.10}$$

where $\mathscr{K}_{rr}$, $\mathscr{K}_{rz}$, $\mathscr{K}_{zr}$ and $\mathscr{K}_{zz}$ are complicated functions of r and r' involving complete elliptic integrals. The detailed forms are given in Appendix C.

We make the problem dimensionless by scaling all lengths with respect to h and all velocities with respect to $g'h^2\rho_+/\mu$, where $g' = g(\rho_- - \rho_+)/\rho_+$. This scaling gives rise to a dimensionless sink strength

$$Q = \frac{q\mu}{\rho_+ g' h^4} \tag{2.11}$$

and a capillary number

$$\Gamma = \frac{\gamma}{\rho_+ g' h^2}. \tag{2.12}$$

These are the only parameters in the dimensionless system. From now on all quantities will be dimensionless unless explicitly stated otherwise. We combine (2.3) and (2.10) to deduce that the total velocity at a point (r, z) lying on the interface $z = f(r)$ is given by

$$\begin{pmatrix} u_r \\ u_z \end{pmatrix} = \frac{Q}{4\pi((1-z)^2+r^2)^{\frac{3}{2}}} \begin{pmatrix} -r \\ 1-z \end{pmatrix} + \frac{1}{8\pi}\int_0^\infty \begin{pmatrix} \mathscr{K}_{rr}f' - \mathscr{K}_{rz} \\ \mathscr{K}_{zr}f' - \mathscr{K}_{zz} \end{pmatrix} F r'\,\mathrm{d}r', \tag{2.13}$$

where $F = f(r') - \Gamma\kappa(r')$ and κ is given by (2.9). This equation forms the basis of the numerical scheme described in §4.

For small values of Q we would expect the interface to assume a stable configuration in which the restoring forces of buoyancy and surface tension balance the advective effects of a weak sink, thus keeping the interface near $z = 0$. As Q increases it will reach a critical value $Q_c(\Gamma)$ beyond which there is no stable interfacial position. When $Q > Q_c(\Gamma)$ we expect the interface to be drawn into the sink and both fluids to be withdrawn.

Before commencing numerical integration of (2.13) to determine Q_c, it is instructive to consider some special cases analytically. These cases, discussed in the following section, shed light on the nature of the interfacial instability for $Q > Q_c$ and provide a useful check of the integration scheme. Discussion of numerical solutions to (2.13) resumes in §4.

3. Interfacial modes and timescales of motion

Consider the situation in which $Q = 0$. If the interface is disturbed away from its equilibrium position at $z = 0$, then the restoring actions of buoyancy and surface tension will cause it to return towards its original position. We find the timescale of the return to equilibrium by considering the eigenmodes of the motion in the case of a small-amplitude perturbation. For simplicity, we initially consider only axisymmetric eigenmodes.

Let the interfacial position be $z = \zeta(r, t)$ with $\zeta \ll 1$ and $\partial\zeta/\partial r \ll 1$. The fluid motion is given by (2.1) subject to the conditions of continuity and stress at the interface. For a small-amplitude perturbation, we may apply these conditions at $z = 0$ rather than at $z = \zeta$, the errors being negligible. We solve (2.1*a*) by introducing the stream function ψ with

$$\boldsymbol{u} = \left(-\frac{\partial\psi}{\partial z}, 0, \frac{1}{r}\frac{\partial}{\partial r}(r\psi)\right). \tag{3.1}$$

The curl of (2.1*b*) produces

$$\left(\nabla^2 - \frac{1}{r^2}\right)^2 \psi = 0. \tag{3.2a}$$

The continuity of velocity and of tangential stress at the interface imply that

$$\left[\frac{\partial\psi}{\partial z}\right]_-^+ = 0, \qquad \left[\frac{\psi}{r} + \frac{\partial\psi}{\partial r}\right]_-^+ = 0, \tag{3.2b, c}$$

$$\left[\frac{\partial}{\partial r}\left(\frac{1}{r}\frac{\partial}{\partial r}(r\psi)\right) - \frac{\partial^2\psi}{\partial z^2}\right]_-^+ = 0, \tag{3.2d}$$

where $[\ ]_-^+$ denotes the jump across $z = 0$. The remaining boundary conditions are the normal-stress balance across the interface,

$$\left[\frac{2}{r}\frac{\partial}{\partial r}\left(r\frac{\partial\psi}{\partial z}\right) - P\right]_-^+ = \Gamma\left(\frac{\partial^2\zeta}{\partial r^2} + \frac{1}{r}\frac{\partial\zeta}{\partial r}\right) - \zeta, \tag{3.2e}$$

where P is determined from (2.1*b*), and the kinematic boundary condition

$$\frac{\partial\zeta}{\partial t} = \frac{\psi}{r} + \frac{\partial\psi}{\partial r}. \tag{3.2f}$$

It is easy to verify that the eigenmodes of the system of equations (3.2) are given by

$$\psi = \mathrm{J}_1(kr)\,(1+kz)\,\mathrm{e}^{-kz-\sigma t} \quad (z>0), \tag{3.3a}$$

$$\psi = \mathrm{J}_1(kr)\,(1-kz)\,\mathrm{e}^{kz-\sigma t} \quad (z<0), \tag{3.3b}$$

and

$$\zeta = \frac{k}{\sigma}\mathrm{J}_0(kr)\,\mathrm{e}^{-\sigma t}, \tag{3.3c}$$

where J_0 and J_1 are Bessel functions of the first kind and of orders 0 and 1. The decay rate σ is given by

$$\sigma = \frac{1}{4}\left(\frac{1}{k}+\Gamma k\right). \tag{3.4}$$

(Though we considered only the axisymmetric eigenmodes for simplicity, it is possible to show that the non-axisymmetric eigenmodes satisfy $\zeta \propto \mathrm{J}_m(kr)\cos(m\theta)\,\mathrm{e}^{-\sigma t}$ and have decay rates that are given by (3.4) independently of the value of m.)

An appreciation of the dependence of the decay rate σ upon the lengthscale k^{-1} of the disturbance in this simple situation is of crucial importance to our understanding of the more general problem described in §2. We see from the form of (3.4) that the decay of a disturbance is due to the effect of surface tension on short lengthscales ($k\to\infty$) and to buoyancy forces on long lengthscales ($k\to 0$). The least-stable disturbance lengthscale ($k=\Gamma^{-\frac{1}{2}}$) has decay rate $\sigma=\frac{1}{2}\Gamma^{\frac{1}{2}}$. It is clear from physical grounds that a decrease in the surface tension will lead to a decrease in the stability of the system. We now see that in the limit of no surface tension ($\Gamma=0$) disturbances on very short lengthscales will have a negligible decay rate.

Equation (3.4) describes the effect of the stabilizing forces on the system. The next stage of our investigation is to include the destabilizing effects of a background advective flow field. We consider first a simple uniform straining motion,

$$\boldsymbol{u} = (-Er, 0, 2Ez) \quad (E>0), \tag{3.5}$$

for which $\zeta=0$ is still an equilibrium position. However, when ζ is perturbed away from zero the situation is somewhat different. Since the Stokes equations are linear, the effect of a background strain (3.5) on the interfacial modes (3.3) is kinematic rather than dynamic; all horizontal lengths are shortened at a rate E and all vertical lengths are extended at a rate $2E$. The eigenmodes (3.3) become self-similar solutions,

$$\psi = A(t)\frac{\sigma(t)}{k(t)}\mathrm{J}_1[k(t)\,r]\,[1+k(t)\,z]\,\mathrm{e}^{-k(t)\,z} \quad (z>0), \tag{3.6a}$$

$$\psi = A(t)\frac{\sigma(t)}{k(t)}\mathrm{J}_1[k(t)\,r]\,[1-k(t)\,z]\,\mathrm{e}^{k(t)\,z} \quad (z<0), \tag{3.6b}$$

$$\zeta = A(t)\,\mathrm{J}_0[k(t)\,r], \tag{3.6c}$$

where

$$\frac{\mathrm{d}k}{\mathrm{d}t} = Ek, \quad \frac{\mathrm{d}A}{\mathrm{d}t} = -\sigma A \tag{3.7a, b}$$

$$\sigma(k) = \frac{1}{4}\left(\frac{1}{k}+\Gamma k\right)-2E. \tag{3.7c}$$

We see that the straining motion has two effects on an interfacial perturbation. First, the lengthscale k^{-1} decreases with time (3.6a) and, secondly, the amplitude A decays

more slowly than (3.4) suggests by an amount $2E$. Therefore, if $E > \frac{1}{4}\Gamma^{\frac{1}{2}}$ there is a range of wavenumbers $k_1 < k < k_2$ centred around $k = \Gamma^{-\frac{1}{2}}$ in which a perturbation will grow rather than decay. Further, if $\Gamma = 0$ then the system is unstable to disturbances on all lengthscales k^{-1} less than $8E$. (We note that if $E < 0$ then the straining motion will be stabilizing rather than destabilizing.)

It is, of course, possible to extend the analysis further. Equations (3.7) may be integrated to find the growth in the amplitude A in the unstable range of wavenumbers ($k_1 < k < k_2$). Alternatively we may wish to consider an interfacial equilibrium of the general problem with a sink above the interface and to analyse the evolution of a wave packet of ripples as it is advected toward the origin. Provided the width of the packet is less than the lengthscale of the flow induced by the sink then (3.7) will still hold, now with E a function of time equal to the local strain rate at the location of the packet. However, such analyses are restricted to infinitesimal perturbations and at this point we move on to discuss the growth of disturbances at finite amplitude, together with the stability of solutions to (2.13).

Consider the situation with a sink ($Q > 0$) above the interface and suppose that there is an equilibrium interfacial position $z = f(r) \neq 0$. The time-development of a general perturbation to this position can only be evaluated numerically. However, the physical processes – buoyancy, surface tension and strain – underlying the time-development have the same effects as in the idealized case of uniform strain on a nearly plane interface. We use the insight gained from that earlier example to construct scaling arguments that describe the behaviour in the present case.

Suppose the interface is disturbed towards the sink with a perturbation of magnitude H and horizontal lengthscale L with $H \leqslant O(L)$. The restoring forces of buoyancy and surface tension are $O(HL^2)$ and $O(\Gamma\kappa L^2)$ respectively, where the curvature κ is $O(H/L^2)$. Under these forces the perturbation tends to subside at a velocity $O(U^{\mathrm{d}})$, which is determined by a balance of the restoring forces and the viscous resistance $O(U^{\mathrm{d}}L)$. Thus U^{d} is $O(H(L+\Gamma/L))$. On the other hand, the portion of the interface displaced towards the sink finds itself in a region of greater sink velocity and tends to move upward. The change U^{s} in the sink velocity due to a small displacement is proportional to the product of the magnitude of the displacement and the local vertical gradient of $\boldsymbol{u}^{\mathrm{s}}$ (defined by (2.3)). Hence U^{s} is $O(HQ)$. Therefore, whether the perturbation grows or decays depends on the competition between the $O(Q)$ growth due to the strain generated by the sink and the $O(L+\Gamma/L)$ decay due to restoring forces. In the previous analytic example this competition is reflected in (3.7*c*). (If a source ($Q < 0$) rather than a sink is present then the strain due to the source would be in such a direction as to augment the effects of the restoring forces and to stabilize the interfacial position further.)

These arguments hold for all perturbations whose magnitude does not greatly exceed their lengthscale. If Q is greater than $O(L+\Gamma/L)$ then a small perturbation will grow to large amplitude. When $H \gg L$ we must replace the estimate of the viscous resistance to restoring forces by $O(U^{\mathrm{d}}H)$ and of κ by $O(1/L)$. We conclude that in this limit U^{d} increases much more slowly than H. Conversely, the gradients of the sink flow increase rapidly as the sink is approached, leading to the conclusion that U^{s} increases rather more rapidly than H. Therefore, we expect that, if Q is sufficiently large for an infinitesimal perturbation to grow, at finite amplitudes the perturbation will continue to grow at an even greater rate.

To summarize, the stabilizing influences of surface tension and gravity have a minimum at a lengthscale that is a decreasing function of Γ. When $\Gamma = 0$ the stabilizing effects are due to gravity alone and are negligible at small lengthscales.

Therefore, as $\Gamma \to 0$ the destabilization due to the gradients of sink flow must eventually dominate on a range of short lengthscales; disturbances on these lengthscales grow increasingly rapidly to large amplitude. The unperturbed interfacial equilibrium thus becomes unstable at a critical value of Γ. Put the other way round, there is a critical value $Q_c(\Gamma)$ such that no stable equilibrium position of the interface exists for $Q > Q_c(\Gamma)$. Furthermore $Q_c(0) = 0$.

We note, finally, that the bifurcation to instability is likely to be subcritical; sufficiently large disturbances from equilibrium towards the sink will lead to simultaneous withdrawal, even if $Q < Q_c$.

4. The numerical scheme

In the previous section we presented arguments that predict a critical value, $Q_c(\Gamma)$, of the flow rate which, if exceeded, produces simultaneous withdrawal of both fluid layers. We now describe a numerical method of solution for (2.13) which allows us to determine the interfacial motion for general values of Q and Γ and, in particular, leads to evaluation of the critical withdrawal rate. The method is similar to previous schemes for the solution of the Stokes equations by means of the boundary-integral representation (2.4) (Youngren & Acrivos 1975; Rallison & Acrivos 1978; Lee & Leal 1982; Geller *et al.* 1986).

Equation (2.13) gives the velocity of points lying in the interface, and hence the rate of change of interfacial position, as an integral function of the current position. The interfacial shape, $z = f(r)$, is represented by 153 points; 20 points are spaced linearly in $0 \leqslant r < 0.1$ and 133 points are spaced in geometric progression with ratio 1.05 in $0.1 \leqslant r \leqslant 65.79\ldots$ (i.e. about 14 points in each interval $r_0 \leqslant r < 2r_0$). This distribution of points is chosen to give an efficient representation of the short lengthscales involved in instability near the sink on the axis and the large lengthscales involved in the overall interfacial shape away from the axis. The spacing of the points varies smoothly in the transition from linear to geometric progression at $r = 0.1$; no anomalous behaviour was detected in this region, nor did the use of a grid with different spacing or another transition point affect the results.

The calculation of the integrals at these values of r requires a discretization with respect to the integration variable r'. The use of the 153 points approximating f is natural. However, when r is small the kernel of the integral is rapidly varying and we must interpolate f to provide sufficient points to give a smooth representation of the integrand. This interpolation and the evaluation of f' and κ is achieved by fitting quartic segments passing through each point and its four nearest neighbours (the first and last two points are treated separately). Further, the velocity produced by a ring of unit Stokeslets at a large radius r' does not tend to zero as $r/r' \to 0$ and the convergence of the integral is due solely to the decay of the strength of the Stokeslet distribution on the interface as $r' \to \infty$. We note that $f = O(r^{-3})$ as $r \to \infty$ (cf. Appendix A) and fit a curve of the form $z = ar^{-3} + br^{-4}$ to represent f in $r > 65.79$. The integration over this range is performed by transformation to a finite range and use of the trapezium rule. In the range $r < 65.79$, the logarithmic singularity of the integrand at $r = r'$ is subtracted and integrated analytically; the remainder is integrated using the trapezium rule.

It is clear that near an interface in equilibrium the fluid velocity at a representative point will be nearly tangential to the interface. Since only the normal component of velocity produces interfacial motion then any multiple of the tangential component can be subtracted and the remainder used in an Euler stepping scheme to calculate

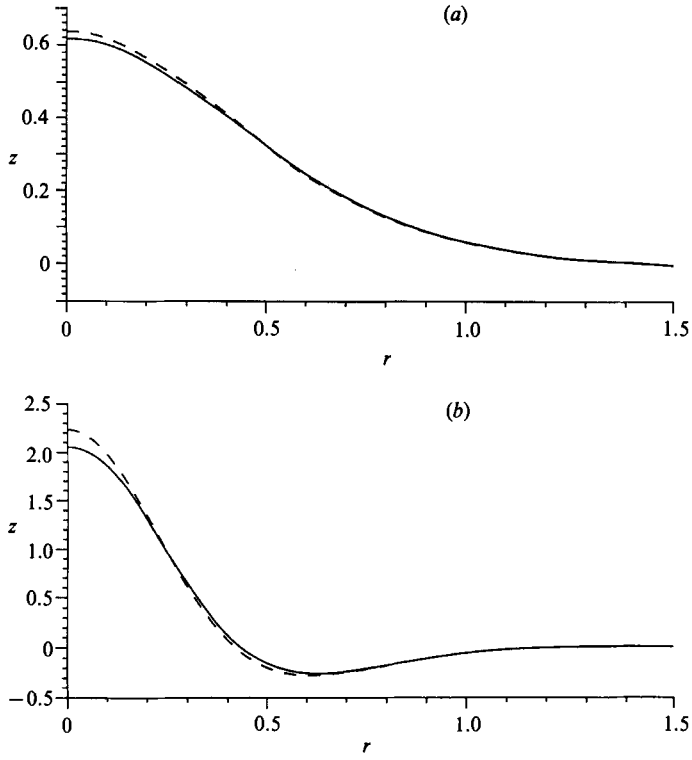

FIGURE 2. Comparison of the numerical solution f^N of (2.13) at $Q = -0.01$ with the asymptotic solution $f \sim Qf_1 + Q^2 f_2 + O(Q^3)$. (*a*) f^N/Q (solid), f_1 (dashed). The difference between the curves is almost entirely due to the $O(Q^2)$ term – graphs of f^N/Q and $f_1 + Qf_2$ are indistinguishable. (*b*) $(f^N - Qf_1)/Q^2$ (solid), f_2 (dashed). Some 80% of the difference between the curves is due to the $O(Q^3)$ term; the remainder is numerical error.

the interfacial position at successive timesteps. This flexibility is used to ensure that the representative points maintain their radial position and are not advected towards $r = 0$. For numerical stability, it is necessary for the timestep to be less than any timescale involved with interfacial motion. In practice, this constraint is equivalent to the timestep being smaller than the timescale associated with the longest lengthscales and the use of too large a timestep leads to a long-wavelength instability.

Though Euler timestepping and the trapezium rule are simple methods of integration, a careful check on the accuracy of the method shows that the use of more sophisticated integration schemes does not justify the increased computational expense. In particular, it is found that runs with small values of Q give excellent agreement with an analytic solution in ascending powers of Q for the velocity field and interfacial shape that is described in Appendix A. Graphs of the theoretical solution to $O(Q^2)$ and the numerical solution at $Q = -0.01$ are shown in figure 2. (Since Q is negative these solutions are stable.) Comparison with solutions at different values of Q allows us to attribute 80% of the small difference between the solutions to the $O(Q^3)$-terms in the series expansion; the remaining 20% of the difference is due to numerical errors. From this we estimate that the numerical errors in the interfacial velocities are less than 0.2% and that the final interfacial positions are accurate to within 1%.

It should be noted that this is an initial-value problem and the motion depends on the initial configuration of the interface. We would expect that if the initial deformation of the interface was sufficiently far from equilibrium and close to the sink then instability would result. The initial configuration used, therefore, was either that of no deformation or that of an equilibrium position at a slightly smaller value of Q, or at a larger value of Γ, for which a stable equilibrium had already been found to exist. This procedure assumes that if a stable equilibrium configuration of the interface exists at a given flow rate then it is unique and may be obtained by a gradual increase in Q from zero. No results were obtained that suggested that this assumption is false.

5. Numerical results

We have seen that the numerical scheme outlined in the previous section produces excellent agreement with the perturbation analysis of Appendix A (see figure 2). In this section we describe results from a numerical investigation of the ideas presented in §3. We calculate the decay timescale of disturbances to an interfacial equilibrium as a function of their lengthscale, discuss the behaviour of the interface in initial-value problems in which Q is suddenly increased from zero, and determine the critical flow rate $Q_c(\Gamma)$.

Equation (3.7c) describes the decay rate of small self-similar perturbations to a flat interface. Now, consider any interfacial equilibrium (found numerically). If $Q < Q_c$ then the equilibrium is stable and we expect a small perturbation to the position of the interface to decay. In particular, at $t = 0$ we add a disturbance of the form

$$\left.\begin{aligned} \Delta z &= \epsilon \cos^2 \frac{\pi r k}{4} \quad (rk < 2) \\ &= 0 \qquad\qquad\quad (rk > 2). \end{aligned}\right\} \tag{5.1}$$

A typical lengthscale for the perturbation at $t = 0$ is given by k^{-1} and a characteristic decay rate is given by $\sigma = \epsilon / u_{z0}$ where u_{z0} is the vertical component of velocity at $r = 0$ and $t = 0$. If the disturbance equations are linear then the value of σ should be independent of ϵ. A value of $\epsilon = 10^{-3}$ was found to be sufficient for this to be the case.

In figure 3 we plot σ against k for three pairs of values of Q and Γ. The results differ in numerical detail from (3.7c) partly because the disturbance is not a self-similar solution and partly because the undisturbed interfacial position is no longer flat. However, the evolution of the perturbation is governed by the processes described by the detailed scaling arguments presented at the end of §3. We find that the qualitative dependence of σ on k and Γ is in agreement with the predictions of these arguments: σ is proportional to k^{-1} as $k \to 0$ and proportional to Γk as $k \to \infty$; the least-stable lengthscale is at $k \approx \Gamma^{-\frac{1}{2}}$ independently of the value of Q and has a decay rate that is an increasing function of Γ and a linearly decreasing function of Q. We deduce that at small values of Γ an interfacial equilibrium is least stable to short-wavelength disturbances and that, as expected, Q_c will be an increasing function of Γ and will tend to zero as $\Gamma \to 0$.

Having confirmed our ideas concerning the decay rate of disturbances to an interfacial equilibrium, we present results from an investigation of the existence of stable equilibria and the determination of the critical flow rate $Q_c(\Gamma)$. In this investigation the following procedure was used. Starting from a stable position (e.g. $Q = 0, f = 0$) the value of Q was increased or the value of Γ was decreased by a small

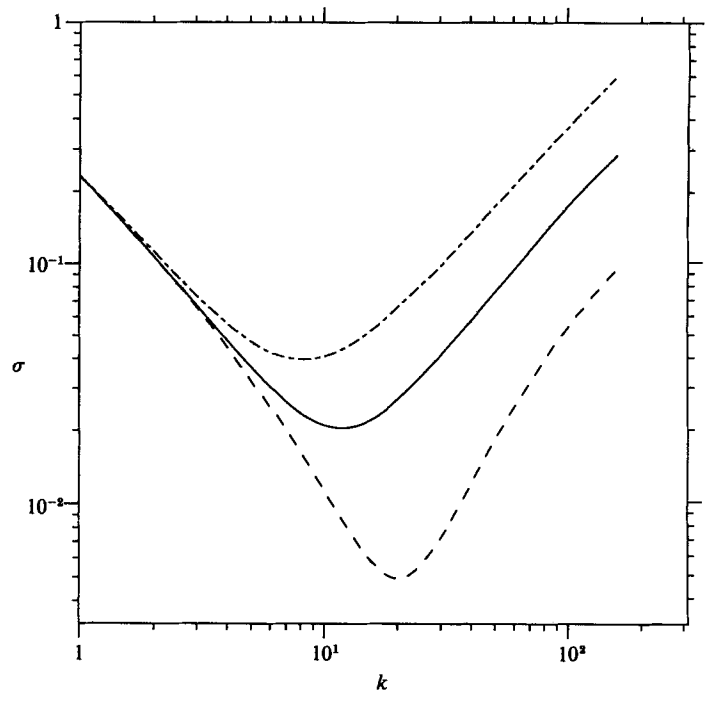

FIGURE 3. The decay rate σ of a small perturbation to an interfacial equilibrium as a function of the wavenumber k of the disturbance. As $k \to \infty, \sigma \propto \Gamma k$; as $k \to 0, \sigma \propto k^{-1}$. Dashed line $Q = 0.08$, $\Gamma = 0.002$; solid line $Q = 0.09, \Gamma = 0.005$; dotted and dashed line $Q = 0.09, \Gamma = 0.010$.

amount. The interfacial motion was integrated numerically until a sustained growth or decay of the upward velocity was observed. We assume that if a stable equilibrium is possible under the new flow conditions then the interfacial position will adjust from its initial value towards this equilibrium, the interfacial velocities ultimately decaying exponentially at the rate of the least-stable lengthscale of perturbation. Conversely, if no stable equilibrium is possible then the interface will be advected towards the sink and the upward interfacial velocity will increase rapidly.

In order to illustrate this dichotomous behaviour, we describe two examples of the evolution of the interfacial shape from an initial planar state. The two cases were chosen to straddle the critical flow curve and gave results that are typical of a stable and an unstable flow condition. Both cases have $Q = 0.08$; they differ in the values of Γ, which are 10^{-3} and 2×10^{-3}. The evolution of the interfacial shape and the upwards velocity at $r = 0$ are shown in figures 4 and 5.

Initially the two solutions are very similar, as would be expected. At the very early stages restoring forces are negligible and the entire interface is advected upwards. As the buoyancy forces increase, the interface approaches equilibrium on the longest (and, by 3.4, most rapidly adjusting) lengthscales; interfacial motion continues on shorter lengthscales in the central region around $r = 0$. From $t \approx 40$ solutions start to diverge as deformation shifts to shorter lengthscales and surface-tension forces become significant. The shift to shorter lengthscales is caused partly because they adjust more slowly (cf. (3.7*c*)) and partly because disturbances are advected to shorter scales (cf. (3.7*a*)). The decreasing width of the growing peak in the interfacial deformation may be seen in figure 4 and can be characterized by the radial position of the inflexion point which decreases with time, in the case $\Gamma = 2 \times 10^{-3}$ from 0.3 at

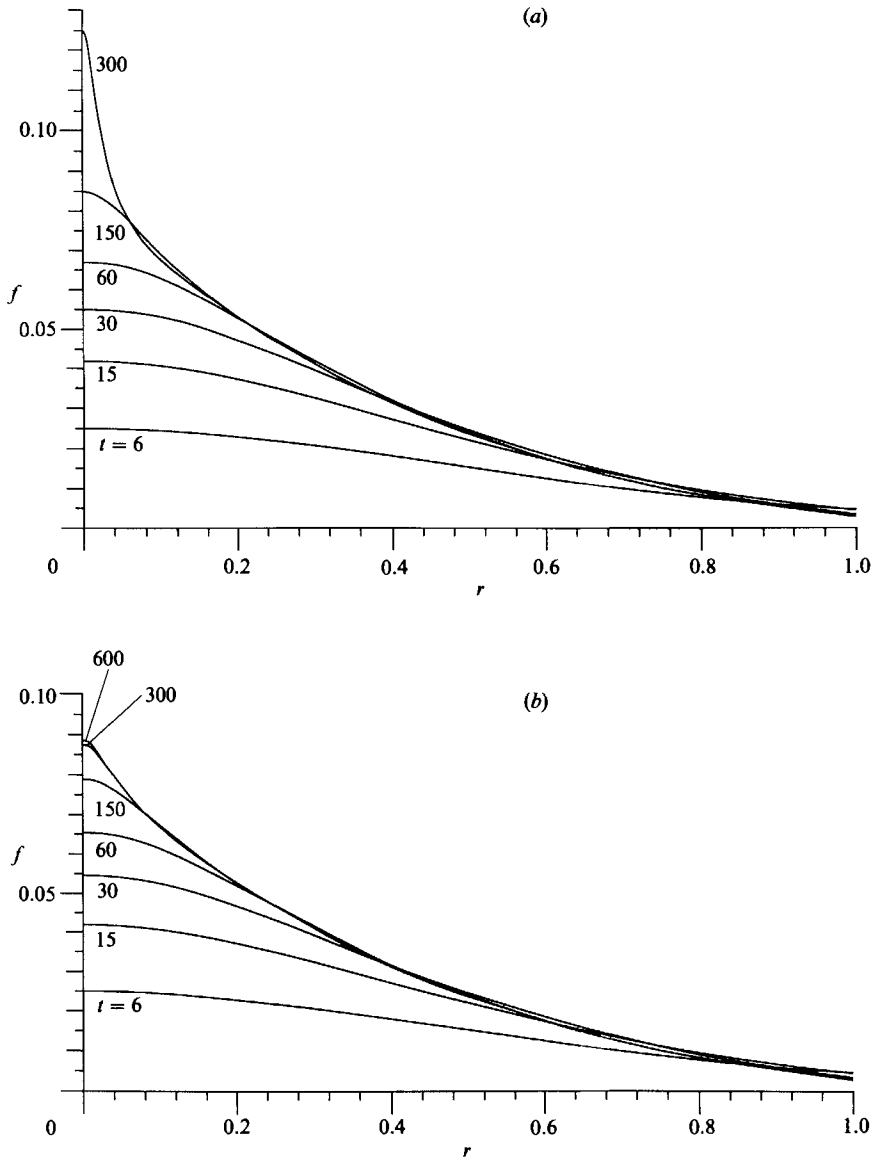

FIGURE 4. The evolution of the interfacial shape $z = f(r, t)$ from planar initial conditions: (*a*) $Q = 0.08, \Gamma = 10^{-3}$; (*b*) $Q = 0.08, \Gamma = 2 \times 10^{-3}$.

$t = 30$ to a limit of 0.03 as $t \to \infty$. From $t = 100$ onwards the difference between the two solutions is increasingly marked. For $\Gamma = 2 \times 10^{-3}$, surface-tension forces are sufficient to limit the growth of the tip of the interfacial peak and interfacial velocities decay rapidly for $t > 250$ as equilibrium is approached. For $\Gamma = 10^{-3}$, on the other hand, surface tension is weaker and the peak continues to be advected towards regions of ever-increasing sink velocities. At large times ($t > 350$) the peak is drawn out into a thin tendril extending towards the sink; the weight of the tendril is insufficient to prevent it from reaching the sink, causing fluid from the lower layer to be withdrawn.

In the above examples the initial conditions were planar and far from equilibrium.

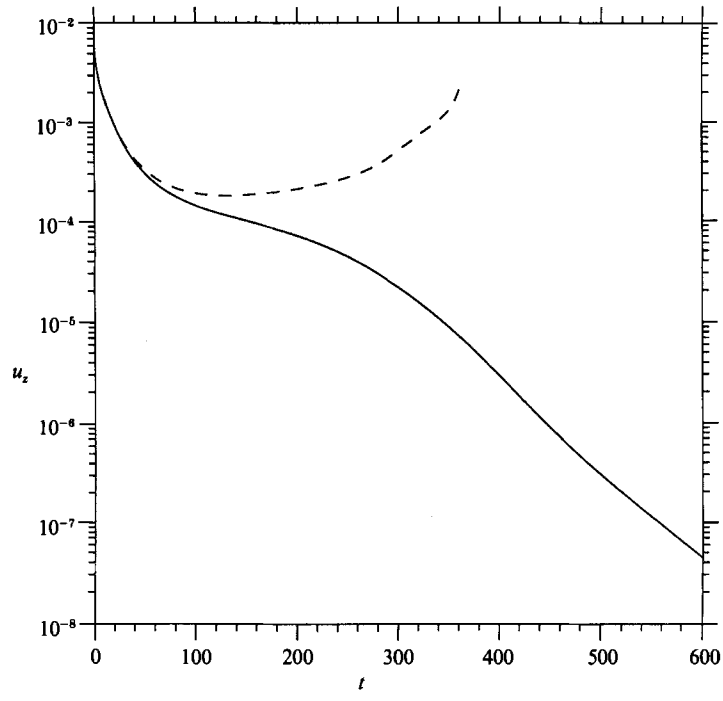

FIGURE 5. The variation of interfacial velocity at $r = 0$ with time: $Q = 0.08, \Gamma = 10^{-3}$ (dashed) and $Q = 0.08, \Gamma = 2 \times 10^{-3}$ (solid).

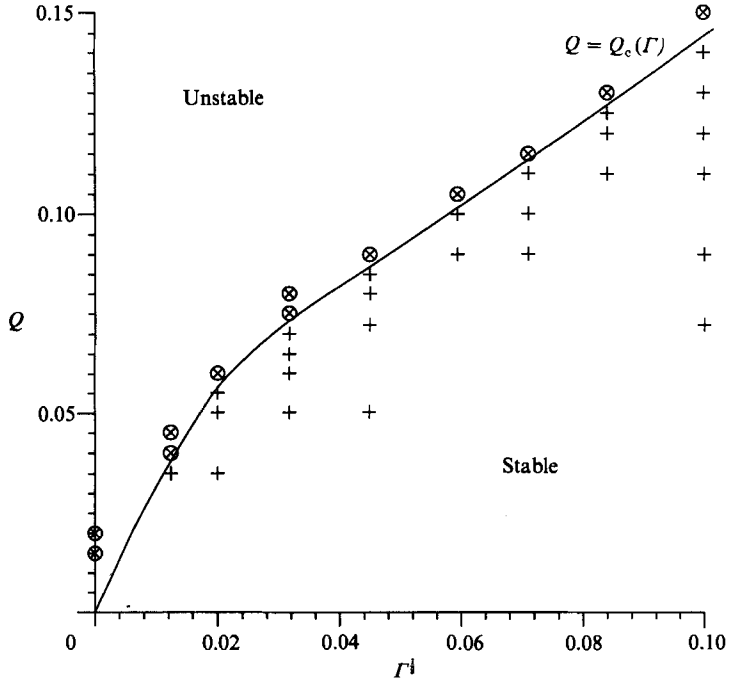

FIGURE 6. Interfacial stability diagram. Points marked + correspond to stable equilibria; points marked ⊗ correspond to instability and withdrawal of the lower layer.

As mentioned before, in the determination of $Q_c(\Gamma)$ less extreme initial conditions were used, each simulation starting from a previously determined and nearby equilibrium. The results of our simulations are shown in the $(Q, \Gamma^{\frac{1}{2}})$-plane in figure 6. The dividing line between the stable and unstable regions is $Q = Q_c(\Gamma)$. As expected, Q_c increases monotonically with Γ from a value very close to zero.

At small values of Γ the calculated critical value of the flow rate may be an overestimate of the true value since the numerical scheme cannot represent instabilities at wavelengths smaller than the grid-point spacing. However, the results for $\Gamma = 0.000\,15$ were unaltered by the use of a numerical grid with twice the density of points as that described in §5. Further refinement of the grid was prohibited by the computational expense. Thus it was not possible to demonstrate that $Q_c(0) = 0$ though no stable configurations were found with $Q > 0$ and $\Gamma = 0$ and we did show that $Q_c(0) < 0.015$.

6. The fluid proportions withdrawn at supercritical flow rates

In the previous section we determined the critical flow rate $Q_c(\Gamma)$ above which simultaneous withdrawal from both layers must occur. We found that, for small values of Γ and hence small values of Q_c, at slightly supercritical flow rates the lower fluid is drawn into the sink through a thin tendril whose weight is insufficient to cause it to fall with a velocity greater than the advective flow towards the sink. In this regime the volume flux from the lower layer will be much less than that from the upper. Here we evaluate the ratio ϕ of the flux of lower fluid to the total flux as a function of the (supercritical) flow rate Q. In this calculation it is possible to make the approximation $\Gamma = 0$ since short-lengthscale disturbances are suppressed by the negative strain rate normal to the interface.

In the immediate neighbourhood of the sink the velocities are large and the assumption of Stokes flow breaks down. In terms of the dimensional variables, inertial forces will be important within a distance $R_i = O(q/\nu)$ of the sink and we assume that ν is sufficiently large that $R_i \ll h$. Sink flow is a solution to the complete Navier–Stokes equations and in the absence of buoyancy forces the streamlines will be everywhere radial to the sink. In a region surrounding the sink, the inwards velocity will dominate any buoyancy-driven motion and the streamlines will still be nearly radial. We assume that this region has radius greater than R_i so that inertial forces are only important in the region where the streamlines are radial. Under this assumption, the direction from which a given streamline enters the sink is prescribed by its behaviour in the region in which Stokes equations are valid. Therefore, we may use (2.13) to determine the equilibrium shape of the interface during steady simultaneous withdrawal.

When the interface passes through the location of the sink the numerical scheme described in §4 requires some modification. Euler timestepping of the interfacial position must be abandoned near the sink since the large velocities cause the timescale of motion to be much shorter than any feasible timestep. Instead, at each iteration the velocity produced by the current interfacial shape is calculated. For a fixed r_E, the portion of the interface lying in $r \geqslant r_E$ is updated, as before, by an Euler timestep using the normal component of the sum of the sink and buoyancy-driven velocities. An approximate streamline passing through the interface at $r = r_E$ is found by integration inwards to the sink with a fourth-order Runge–Kutta scheme using the buoyancy-driven velocity of the old interfacial position and the sink velocity at each point on the streamline. (The approximation lies in using the

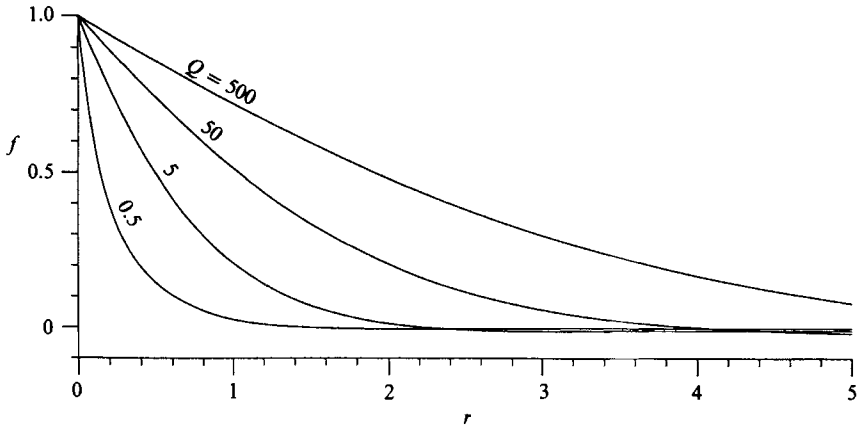

FIGURE 7. Interfacial shapes $z = f(r)$ during steady simultaneous withdrawal at supercritical flow rates Q.

buoyancy-driven velocity on the interface and not on the streamline.) The interface lying in $r \leqslant r_E$ is updated to lie on this streamline.

Though this scheme loses the link between iteration and time-development it serves our purpose of finding the equilibrium withdrawal position. First, in the equilibrium position the interface coincides with a streamline and successive iterations coincide. Secondly, if the interfacial position is higher (lower) than equilibrium at one iteration then the buoyancy-driven flow will be larger (smaller), streamlines will cross the interface downwards (upwards) as r decreases and the interfacial position will be corrected downwards (upwards) towards equilibrium at the next iteration. Provided r_E is sufficiently far from the sink to ensure numerical stability, the choice of r_E should not and did not affect the computed equilibrium position.

From the equilibrium position of the interface it is a simple matter to calculate the flux ratio ϕ since it is equal to the fraction of total solid angle occupied by the lower fluid within the region of radial inflow near the sink. Let

$$\tan\theta = -\lim_{r\to 0} \frac{\mathrm{d}f}{\mathrm{d}r}. \tag{6.1}$$

Then

$$\phi = \frac{1-\sin\theta}{2}. \tag{6.2}$$

As a check on the numerical results it is instructive to consider the limit $Q \gg 1$. In equilibrium the components of the sink and buoyancy-driven flows normal to the interface must balance. As Q increases, the deformation of the interface required to produce a buoyancy-driven flow that balances the vertical component of the sink flow also increases. Hence ϕ is an increasing function of Q. As $Q \to \infty$ (an equivalent dimensional limit is $h \to 0$) the region in which buoyancy is negligible and the flow is radial grows and so $\theta \to 0$ and $\phi \to \frac{1}{2}$, i.e. fluid is withdrawn equally from the two layers. Suppose the horizontal scale of interfacial deformation is $L \gg 1$. The typical vertical component of velocity due to the deformation has magnitude $O(L)$ and must

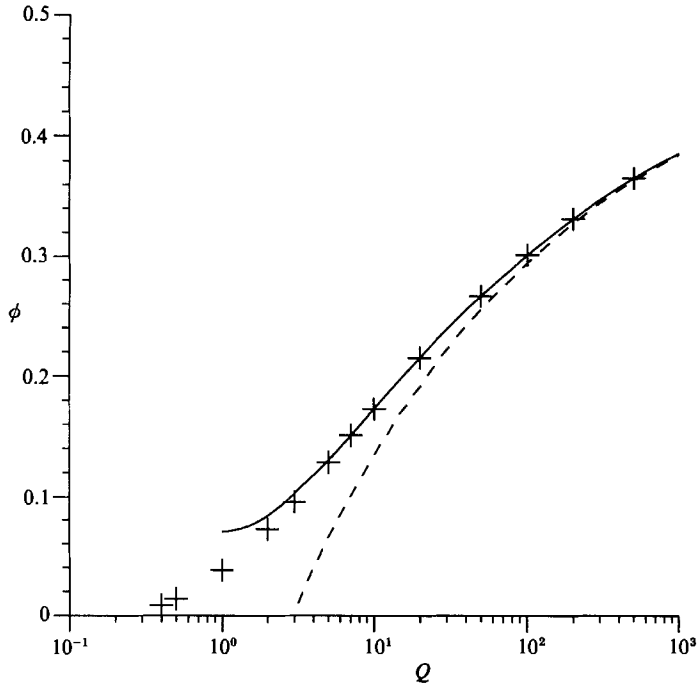

FIGURE 8. The flux ratio ϕ of lower fluid to total fluid withdrawn at supercritical flow rates Q. Points marked + are the calculated values; the dashed curve $\phi = \frac{1}{2} - 0.654Q^{-\frac{1}{4}}$ and the solid curve $\phi = \frac{1}{2} - 0.654Q^{-\frac{1}{4}} + 0.224Q^{-\frac{3}{4}}$ are asymptotic solutions as $Q \to \infty$.

balance that due to the sink, which is $O(Q/L^3)$. Therefore $L \sim Q^{\frac{1}{4}}$. But $\mathrm{d}f/\mathrm{d}r \sim 1/L$ so, from (6.1) and (6.2),

$$\phi = \tfrac{1}{2} - O(Q^{-\frac{1}{4}}) \quad \text{as} \quad Q \to \infty. \tag{6.3}$$

A full asymptotic expansion as $Q \to \infty$ is likely to be in inverse powers of $Q^{\frac{1}{4}}$.

Some equilibrium interfacial positions are shown in figure 7. As we expect, the regions of radial flow and the proportion of lower-layer fluid drawn up by the sink both increase with Q. The flux ratio ϕ is shown in figure 8 over the range $0.4 \leqslant Q \leqslant 500$. The results at large Q are in agreement with (6.3) and are well represented by

$$\phi = \tfrac{1}{2} - 0.654Q^{-\frac{1}{4}} + 0.224Q^{-\frac{3}{4}} \tag{6.4}$$

for $Q \geqslant 5$. For $Q \leqslant 0.4$ the numerical grid was unable to resolve the fine-scale structure of the narrow thread of lower fluid drawn into the sink. Future work with grid points spaced by interfacial arclength, rather than by radial position, will overcome this difficulty.

7. Discussion

Analytic arguments and numerical experiments have been used to investigate the effects of surface tension on the critical flow rate for selective withdrawal from a viscous two-layer system. We find that the system is characterized by the dimensionless flow rate Q and the capillary number Γ. The decay of disturbances to

an equilibrium position of the interface at a subcritical flow rate is dominated by surface tension on small lengthscales and by buoyancy effects on large lengthscales. Hence, both the decay rate and the lengthscale of the least-stable disturbance are increasing functions of Γ. The critical flow rate, above which no stable equilibrium withdrawal of a single layer is possible, is found to be an increasing function of Γ and tends to zero in the limit of no surface tension. We conclude that interfacial tension, however weak, must play a role in stabilizing short-wavelength disturbances if selective withdrawal of a single layer is to be possible.

These conclusions should be compared with the experimental results of Blake & Ivey (1986). They allowed a two-layer system to drain through a hole in the base of its container at constant flow rate, and measured the depth of the lower layer at which the effluent had a composition containing at least 2.5% of upper layer fluid. This was used as a criterion for draw-down. Surface tension was ignored and the data scaled to give an estimate for the critical flow rate of $Q_c = 0.03$. If surface tension were indeed negligible ($\Gamma < 8 \times 10^{-5}$) then, at least according to our results, this is a surprisingly large value of Q (or small value of h) for draw-down to first occur. However, experimental conditions in which the interface is falling and the sink–interface distance consequently decreasing are only quasi-steady and it is necessary to compare the slow growth rate of the short-wavelength instabilities at small capillary numbers with the timescale of the decrease in depth. We also note that, at the onset of draw-down, withdrawal of the lower fluid occurs in a thin thread at small fluxes and would be difficult to observe. Indeed, the experimental observations are not of Q_c but of the value of Q at which $\phi = 0.025$.

Further light may be shed on the mechanism of instability and on the form of withdrawal at slightly supercritical flow rates by comparison with investigations into the bursting of viscous droplets immersed in another fluid undergoing extension. In these studies, reviewed by Rallison (1984), it is found that the equilibrium deformation of a drop increases with the rate of extension and that if the rate of extension exceeds a critical value then no equilibrium is possible, the drop is greatly stretched and breaks up into smaller droplets. Expressed in the non-dimensional units used in this paper, no equilibrium exists for a drop of radius a in strain E if $4\pi Ea/\Gamma > 0.65$ (Rallison & Acrivos 1978). In the selective withdrawal problem there is a stagnation point and extensional flow at the peak $(0, f(0))$ of any subcritical interfacial equilibrium. On sufficiently short lengthscales the velocities produced by buoyancy forces are negligible and the tip of the interfacial peak would be expected to behave in a manner analogous to a fluid droplet; the equivalent critical parameter would be $2Qa/(\Gamma(1-f(0))^3)$, where a scales with the radius of the tip.

The behaviour of the interface at slightly supercritical flow rates may also be likened to that of a fluid droplet. When a relatively inviscid droplet is in strong strain it adopts a spindle shape with conical ends (Taylor 1964) from which small droplets are emitted by 'tip-streaming'. Here, since the fluids are of equal viscosity, we expect that, as was observed numerically, a rounded interfacial tip is greatly extended into a filament drawn towards the sink. It is possible either that capillary instabilities would cause the filament to break up into droplets or that the extension of the filament would suppress the instabilities and allow the filament to be drawn into the sink intact (Tomatiko 1936; Mikami, Cox & Mason 1975). It is hoped that this issue may be resolved by extension to smaller values of Q of the calculations of the flux ratio ϕ described in §7. If we regard Q as a function of ϕ then $\lim_{\phi \to 0_+} Q \leqslant Q_c$ would tend to indicate that the filament reaches the sink resulting in steady withdrawal, whereas $\lim_{\phi \to 0_+} Q > Q_c$ would indicate that there is a range of flow rates in which

intermittent withdrawal occurs by a succession of filaments being broken into droplets.

In this paper we have considered the simplest geometry possible in order to isolate the effects of interfacial tension on the stability of subcritical interfacial equilibria and on the critical flow rate. This approach promotes the understanding of the physical processes involved and aids the design and interpretation of more complex models. In any experimental or practical application to withdrawal from a container, the effect of the rigid container walls and of the finite dimensions of the orifice must also be taken into account. Such effects could be investigated numerically using the techniques of this paper by modifying the basic sink flow and including the integrals involving the stresses on the walls of the container in the boundary-integral representation. A wall in the neighbourhood of the sink would be expected to focus the withdrawal in the direction normal to the wall (Blake & Chwang 1974) and to increase the likelihood of simultaneous withdrawal. Further development should include the effects of unequal viscosities, as described in Appendix B, and investigate the sensitivity of the flux ratio ϕ to the viscosity ratio. It may also be instructive to consider the effects of variations of Q on timescales shorter than or comparable with the timescale for adjustment to interfacial equilibrium.

The application of our results to the tapping of layered magma chambers is of particular interest. As described above, direct quantitative application of our analysis to magma chambers is inappropriate since the effects of the chamber walls and of any viscosity stratification will modify the numerical details of the results. The qualitative results will, however, be relevant owing to the same underlying physical processes.

Eruption conditions vary enormously and both simultaneous and sequential withdrawal of the layers have been observed. If simultaneous tapping of two layers occurs then theoretical calculations show that the two-phase flow in the conduit will be unstable (Hickox 1971; Joseph, Renardy & Renardy 1984). Experimental studies confirm this and show that substantial mixing of the magmas will occur (Koyaguchi 1985; Freundt & Tait 1986); this mechanism has been proposed for the formation of banded pumice. The composition and texture of the eruption products can thus vary greatly according to whether selective withdrawal does or does not take place. The composition of the outflow will, therefore, depend on the flow rate and on the layer structure and geometry of the chamber as well as on the composition of the chamber contents and the amount of contamination during ascent. Recent finite-element simulations of eruption from an idealized magma chamber with arbitrary initial density and viscosity stratification show that the effects of these parameters are complex (Spera *et al.* 1986). However, such simulations are computationally very expensive at resolutions of less than tens of metres and it seems clear that further fundamental research is necessary if field geologists are to be able to invert observed eruptive compositional profiles to deduce the pre-eruptive stratification in the chamber.

I would like to thank H. E. Huppert and M. G. Worster for their constructive comments. Financial support from the Natural Environment Research Council is gratefully acknowledged.

Appendix A. The equilibrium of a nearly flat interface

In this appendix we derive an expression for the equilibrium interfacial condition $z = f(r)$ that is valid in the limit of a weak sink ($Q \ll 1$). In such an equilibrium we expect the $O(Q)$ advective flow towards the sink to be balanced by the surface-tension and buoyancy forces produced by an $O(Q)$ deformation of the interface from its flat position. We seek, therefore, a solution of the form

$$f \sim Qf_1 + Q^2 f_2 + O(Q^3), \tag{A 1a}$$

$$\boldsymbol{u} \sim Q\boldsymbol{u}_1 + Q^2\boldsymbol{u}_2 + O(Q^3), \tag{A 1b}$$

$$P \sim QP_1 + Q^2 P_2 + O(Q^3), \tag{A 1c}$$

where the leading-order velocity $\boldsymbol{u}_1$ includes the sink flow that forces the solution to be non-zero.

The Stokes flow $(\boldsymbol{u}, P)$ must satisfy boundary conditions at $z = f$ comprising continuity of velocity and of tangential stress, a discontinuity of normal stress equal to $f - \Gamma\kappa$ and the kinematic condition that the flow must be tangential to the interface. These conditions may be written in (r, z)-coordinates as

$$[u_r]_{f_-}^{f_+} = 0, \quad [u_z]_{f_-}^{f_+} = 0, \tag{A 2a, b}$$

$$\left[\frac{\partial u_r}{\partial z} + \frac{\partial u_z}{\partial r} - \frac{\mathrm{d}f}{\mathrm{d}r}\left(2\frac{\partial u_r}{\partial r} - P\right)\right]_{f_-}^{f_+} = -\frac{\mathrm{d}f}{\mathrm{d}r}F, \tag{A 2c}$$

$$\left[2\frac{\partial u_z}{\partial z} - P - \frac{\mathrm{d}f}{\mathrm{d}r}\left(\frac{\partial u_r}{\partial z} + \frac{\partial u_z}{\partial r}\right)\right]_{f_-}^{f_+} = F, \tag{A 2d}$$

$$u_z - \frac{\mathrm{d}f}{\mathrm{d}r}u_r = 0 \quad \text{at} \quad z = f, \tag{A 2e}$$

where

$$F = f - \Gamma\left(\frac{\mathrm{d}^2 f/\mathrm{d}r^2}{(1 + (\mathrm{d}f/\mathrm{d}r)^2)^{\frac{3}{2}}} + \frac{\mathrm{d}f/\mathrm{d}r}{r(1 + (\mathrm{d}f/\mathrm{d}r)^2)^{\frac{1}{2}}}\right) \tag{A 2f}$$

and $[\ ]_{f_-}^{f_+}$ denotes the jump from values at $z = f_-$ to values at $z = f_+$. As yet this is still a free-boundary-value problem, so we replace values at $z = f$ by their Taylor expansion about $z = 0$. We substitute from (A 1) and solve at successive orders.

At $O(Q)$ we obtain the following leading-order problem:

$$[u_{1r}]_{-}^{+} = 0, \quad [u_{1z}]_{-}^{+} = 0, \tag{A 3a, b}$$

$$\left[\frac{\partial u_{1r}}{\partial z} + \frac{\partial u_{1z}}{\partial r}\right]_{-}^{+} = 0, \quad \left[2\frac{\partial u_{1z}}{\partial z} - P_1\right]_{-}^{+} = F_1, \tag{A 3c, d}$$

$$u_{1z} = 0 \quad \text{at} \quad z = 0, \tag{A 3e}$$

where $[\ ]_{-}^{+}$ denotes the jump from values at $z = 0_-$ to values at $z = 0_+$ and

$$F_1 = f_1 - \Gamma\left(\frac{\mathrm{d}^2 f_1}{\mathrm{d}r^2} + \frac{1}{r}\frac{\mathrm{d}f_1}{\mathrm{d}r}\right). \tag{A 3f}$$

Thus $\boldsymbol{u}_1$ is the Stokes flow caused by a sink of strength Q at $(0, 1)$ and a Stokeslet distribution $F_1\boldsymbol{e}_z$ on $z = 0$; F_1 is prescribed by the condition that there is no flow

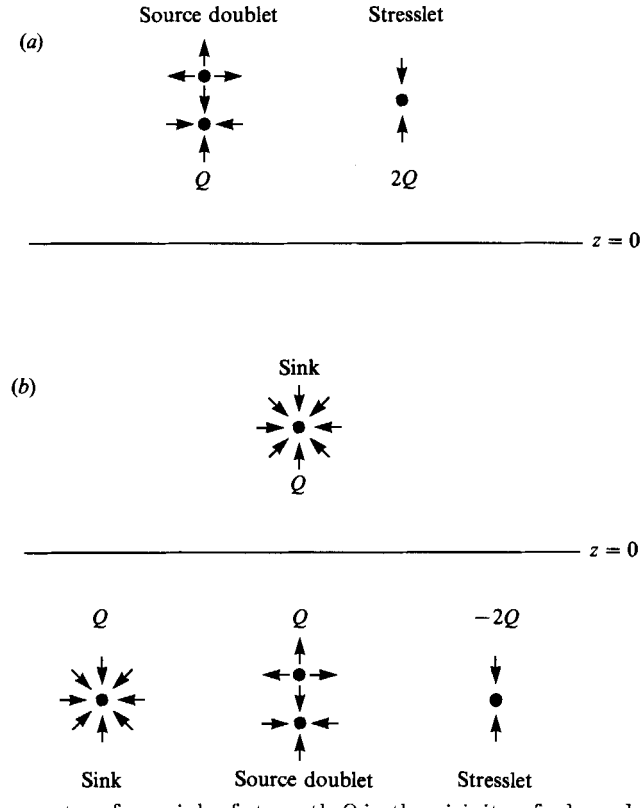

FIGURE 9. The image system for a sink of strength Q in the vicinity of a boundary that is held at $z = 0$ between two fluids of equal viscosity. (*a*) The image system for the flow in $z < 0$. (*b*) The image system for the flow in $z > 0$.

across the plane $z = 0$. Equations (A 3) may be solved for F_1 using the following adaptation by Lee, Chadwick & Leal (1979) of the solution of Lorentz (1907) for motion in the presence of a rigid wall.

If $(\boldsymbol{u}, p)$ is a Stokes flow in an unbounded domain, then the functions

$$\boldsymbol{u}_- = \tfrac{1}{2}(\boldsymbol{u}-\hat{\boldsymbol{u}}), \quad p_- = \tfrac{1}{2}(p-\hat{p}) \qquad (z < 0) \qquad (\text{A } 4a)$$

$$\boldsymbol{u}_+ = \boldsymbol{u}+\tfrac{1}{2}(\boldsymbol{u}^*+\hat{\boldsymbol{u}}^*), \quad p_+ = p+\tfrac{1}{2}(p^*+\hat{p}^*) \qquad (z > 0) \qquad (\text{A } 4b)$$

satisfy (2.1), $\boldsymbol{u}\cdot\boldsymbol{n} = 0$ on $z = 0$, and the conditions of continuity of the tangential components of velocity and stress on $z = 0$. Here $(\hat{\boldsymbol{u}}, \hat{p})$ is the associated solution of Lorentz (1907) given by

$$\left.\begin{aligned} \hat{u}_i &= -u_i + 2\delta_{i3}\,u_3 - 2z\frac{\partial u_3}{\partial x_i} + z^2\frac{\partial p}{\partial x_i}, \\ \hat{p} &= p + 2z\frac{\partial p}{\partial z} - 4\frac{\partial u_3}{\partial z}, \end{aligned}\right\} \qquad (\text{A } 5a)$$

and $(\boldsymbol{u}^*, p^*)$ is the reflected solution given by

$$u_i^* = u_i(x, y, -z) - 2\delta_{i3}\,u_3(x, y, -z), \quad p^* = p(x, y, -z). \qquad (\text{A } 5b)$$

We substitute the sink flow $\boldsymbol{u}^s$ for $\boldsymbol{u}$ in (A 4) and (A 5) to deduce the flow $\boldsymbol{u}_1$ satisfying (A 3*a–c*) and (A 3*e*). It may be shown that $\boldsymbol{u}_1$ is equivalent to the following image system (figure 9), where $\boldsymbol{e}_z$ denotes the unit vector in the z-direction: the flow $\boldsymbol{u}_{1-}$ (in

$z < 0$) is equivalent to a source doublet of strength $Q\boldsymbol{e}_z$ and a stresslet of strength $2Q\boldsymbol{e}_z\boldsymbol{e}_z$ at $z = 1, r = 0$; the flow $\boldsymbol{u}_{1+}$ (in $z > 0$) is equivalent to the sink of strength Q at $z = 1, r = 0$, and an image sink of strength Q, source doublet of strength $Q\boldsymbol{e}_z$ and stresslet of strength $-2Q\boldsymbol{e}_z\boldsymbol{e}_z$, all at $z = -1, r = 0$.

From the solution for $\boldsymbol{u}_1$ we can deduce that the discontinuity F_1 in the normal stress at the interface is given by

$$F_1 = \frac{2-r^2}{\pi(1+r^2)^{\frac{5}{2}}}. \tag{A 6}$$

We conclude that the leading-order interfacial shape is given by $z = f_1(r)$, where f_1 is the solution of

$$\left.\begin{aligned} f_1 - \Gamma\left(\frac{\mathrm{d}^2 f_1}{\mathrm{d}r^2} + \frac{1}{r}\frac{\mathrm{d}f_1}{\mathrm{d}r}\right) &= \frac{2-r^2}{\pi(1+r^2)^{\frac{5}{2}}}, \\ f_1 \to 0 \quad \text{as} \quad r \to \infty, \qquad & f_1(0) \text{ finite.} \end{aligned}\right\} \tag{A 7}$$

If $\Gamma \ll 1$ we can make the further approximation that

$$f_1(r) = \frac{2-r^2}{\pi(1+r^2)^{\frac{5}{2}}} + O(\Gamma). \tag{A 8}$$

After the discussion of §3, we should note that if $Q > 0$ then we need $\Gamma > 0$ for this equilibrium to be stable. If, instead of a sink, we consider a source ($Q < 0$) then the system is always stable and we may put $\Gamma \equiv 0$.

At the next order in the expansion (A 1) the $O(Q^2)$-terms $\boldsymbol{u}_2$, P_2 and f_2 are forced by the quadratic terms in $\boldsymbol{u}_1$, P_1 and f_1 generated by deformation of the interface from its planar position. It is surprising how many of these terms, which appear in the Taylor expansion of (A 2), are zero by virtue of (A 3) and the fact that $(\boldsymbol{u}_1, P_1)$ is a Stokes flow. After these simplifications the resulting problem takes the form

$$[u_{2r}]^+_- = 0, \quad [u_{2z}]^+_- = 0, \tag{A 9a, b}$$

$$\left[\frac{\partial u_{2r}}{\partial z} + \frac{\partial u_{2z}}{\partial r}\right]^+_- = f_1\frac{\mathrm{d}F_1}{\mathrm{d}r}, \quad \left[2\frac{\partial u_{2z}}{\partial z} - P_2\right]^+_- = F_2, \tag{A 9c, d}$$

$$u_{2z} = \frac{1}{r}\frac{\partial}{\partial r}(r u_{1r} f_1) \quad \text{at} \quad z = 0, \tag{A 9e}$$

where

$$F_2 = f_2 - \Gamma\left(\frac{\mathrm{d}^2 f_2}{\mathrm{d}r^2} + \frac{1}{r}\frac{\mathrm{d}f_2}{\mathrm{d}r}\right). \tag{A 9f}$$

Thus $\boldsymbol{u}_2$ is the flow generated by a Stokeslet distribution $f_1(\mathrm{d}F_1/\mathrm{d}r)\boldsymbol{e}_r + F_2\boldsymbol{e}_z$ on $z = 0$; F_2 is specified by the requirement that (A 9e) be satisfied. For the purposes of finding f_2 we may ignore the flow induced by the radial stress distribution since it contains no component across the plane $z = 0$. We are then reduced to the problem of finding the stress distribution F_2 that will produce the given normal velocity on $z = 0$.

A general solution for Stokes flow as a function of the velocity on the boundary of a half-space is derived by Jansons & Lister (1988). This solution may be used to calculate F_2 and then (A 9f) may be solved for f_2. As in the solution of (A 8) we note that if $\Gamma \ll 1$ then $f_2 \sim F_2 + O(\Gamma)$. In that limit also

$$u_{2z} = \frac{1}{2\pi^2}\frac{2r^4 - 9r^2 + 1}{(1+r^2)^5} + O(\Gamma). \tag{A 10}$$

The interfacial form (A 1a) provides a useful check on the accuracy and validity of the numerical scheme described in §4. As we would expect, the $O(Q^3)$-correction is greatest near $r = 0$ where the interfacial shape is most non-planar.

Appendix B. The case of unequal viscosities

The results given previously were derived under the simplifying assumption that the upper and lower fluid layers had equal viscosity μ. Suppose now that the upper fluid has viscosity μ_+ and the lower fluid viscosity μ_-. In this appendix we indicate the modifications necessary to include the dependence on the viscosity ratio $\lambda = (\mu_-/\mu_+)$.

Consider the potential representation of Stokes flow (2.4b). We multiply this identity by the viscosity and apply it to $\boldsymbol{u}^{\mathrm{d}}$ in the domains $z > f$ and $z < f$ as before. We deduce that

$$\frac{\mu_+ + \mu_-}{2} u_i^{\mathrm{d}}(\boldsymbol{x}) = \frac{1}{8\pi} \int \left(\frac{\delta_{ij}}{|\boldsymbol{r}|} + \frac{r_i r_j}{|\boldsymbol{r}|^3} \right) F_j \, \mathrm{d}A(\boldsymbol{y}) + \frac{3(\mu_- - \mu_+)}{4\pi} \int \frac{r_i r_j r_k}{|\boldsymbol{r}|^5} u_j^{\mathrm{d}} n_k \, \mathrm{d}A(\boldsymbol{y}), \quad \text{(B 1)}$$

where F_j must now also include the jump in the stress associated with the sink flow (2.3) caused by the viscosity difference. Thus

$$\boldsymbol{F} = ((\rho_- - \rho_+) g' f - \gamma\kappa)\, \boldsymbol{n} + \frac{q(\mu_+ - \mu_-)}{4\pi R^5} (R^2 \boldsymbol{n} - 3(\boldsymbol{n} \cdot \boldsymbol{R})\, \boldsymbol{R}). \quad \text{(B 2)}$$

We make the problem dimensionless, using μ_+ as the viscosity scale and defining $Q = q\mu_+/(g'\rho_+ h^4)$. The azimuthal integral can again be evaluated using the axisymmetry of the problem. In dimensionless form the resultant equation for the velocity of points lying in the interface is

$$\frac{1+\lambda}{2} u_i(\boldsymbol{x}) + \frac{3(1-\lambda)}{4\pi} \int_0^\infty \mathscr{L}_{ijk} u_j n_k r' \, \mathrm{d}r' = -\frac{QR_i}{4\pi R^3} + \frac{1}{8\pi} \int_0^\infty \mathscr{K}_{ij} F_j r' \, \mathrm{d}r', \quad \text{(B 3)}$$

where

$$\boldsymbol{F} = (f - \Gamma\kappa)\, \boldsymbol{n} + \frac{Q(1-\lambda)}{4\pi R^5} (R^2 \boldsymbol{n} - 3(\boldsymbol{n} \cdot \boldsymbol{R})\, \boldsymbol{R}), \quad \text{(B 4)}$$

$\boldsymbol{R} = (r, 0, 1-z)$, $\boldsymbol{n} = (f', 0, -1)$ and $\mathscr{L}_{ijk}(r'; r)$ and $\mathscr{K}_{ij}(r'; r)$ can be expressed in terms of complete elliptic integrals.

The important difference between (B 3) and the analogous equation (2.13) is that the interfacial velocity is not given explicitly when $\lambda \neq 1$ since it appears in the integral on the left-hand side of (B 3). The discretized version of this equation would take the form of a set of simultaneous linear equations for the velocities of the data points. The matrix-inversion problem is reasonably well conditioned, especially when $\lambda \approx 1$, since $\mathscr{L}_{ijk}$ is peaked at $r = r'$ and the linear system is thus diagonally dominant. However, accurate integration of (B 3) will be computationally expensive.

We can see from (B 3) that the problem of withdrawal from two layers of differing viscosities is characterized by the dimensionless flow rate Q, the capillary number Γ and the viscosity ratio λ. Withdrawal of both layers will occur if $Q > Q_{\mathrm{c}}(\Gamma, \lambda)$ where $Q_{\mathrm{c}}(\Gamma, 1)$ is given in figure 6. Experimental work by Blake & Ivey (1986) suggests that Q_{c} is only weakly dependent on λ and it would be interesting to solve (B 3) to confirm this.

It is important to realize that the underlying physics of the flow does not depend on the assumption $\lambda = 1$ and that the arguments of §3 will carry over to the case

$\lambda \neq 1$. There is a consequent prediction of instability at short lengthscales when $\Gamma \ll 1$, though the numerical details will depend on λ. The case $\lambda \ll 1$ is of interest for those magmatic bodies in which a viscous granitic melt overlies a less viscous basaltic melt.

Appendix C. The azimuthal integral

Let $z = f(r)$ and $z' = f(r')$. Then, in cylindrical polar coordinates (r, θ, z), we find that $\boldsymbol{n}\,\mathrm{d}A = (f', 0, -1)\,\mathrm{d}\theta r'\,\mathrm{d}r'$. Using identities derived from those given by Lee & Leal (1982), it may be shown that the integration over θ in (2.5) leads to (2.10) in which

$$\tfrac{1}{4}C(\mathscr{K}_{zr}f' - \mathscr{K}_{zz}) = (z-z')\left(\frac{(r-r')f' - (z-z')}{A^2 - B^2}\mathrm{E} + \frac{rf'(\mathrm{E}-\mathrm{K})}{B^2}\right) - \mathrm{K}, \tag{C 1a}$$

$$\tfrac{1}{4}C(\mathscr{K}_{rr}f' - \mathscr{K}_{rz}) = (r-r')\left(\frac{(r-r')f' - (z-z')}{A^2 - B^2}\right)\mathrm{E} + f'(\mathrm{K}-3\mathrm{E}) + \frac{(2(z-z')^2 + (r-r')^2)f' - r'(z-z')}{B^2}(\mathrm{K}-\mathrm{E}), \tag{C 1b}$$

where $A^2 = (z-z')^2 + r^2 + r'^2$, $B^2 = 2rr'$, $C^2 = A^2 + B^2$ and $\mathrm{K}(m)$ and $\mathrm{E}(m)$ are complete elliptic functions of the first and second kinds with arguments $m = 2B^2/C^2$.

The form of these equations shows that the singularity as $r' \to r$ is no worse than the logarithmic singularity of the complete elliptic functions as their argument tends to 1. Indeed

$$\left.\begin{aligned} \mathscr{K}_{zr}f' - \mathscr{K}_{zz} &\sim -\frac{2}{r}\mathrm{K} \\ \mathscr{K}_{rr}f' - \mathscr{K}_{rz} &\sim \frac{2}{r}(\mathrm{K}-3\mathrm{E}) \end{aligned}\right\} \quad \text{as} \quad r' \to r, \tag{C 2}$$

and the singularity can thus be subtracted and integrated analytically.

Except when $m \ll 1$, the values of the elliptic functions in (C 1) are calculated using polynomial approximations accurate to within 2×10^{-8} (Abramowitz & Stegun 1965, equations 17.3.34 and 17.3.36). When $m \ll 1$, the Taylor series for E and K (Abramowitz & Stegun 1965, equations 17.3.11 and 17.3.12) are used to avoid the large numerical round-off errors involved in evaluating $\mathrm{E}-\mathrm{K}$ directly.

REFERENCES

Abramowitz, M. & Stegun, I. A. 1965 *Handbook of Mathematical Functions*. Dover.

Bear, J. & Dagan, G. 1964 Some exact solutions of interface problems by means of the hodograph method. *J. Geophys. Res.* **69**, 1563–1572.

Blake, J. R. & Chwang, A. T. 1974 Fundamental singularities of viscous flow. Part 1: the image systems in the vicinity of a stationary no-slip boundary. *J. Engng Maths* **8**, 23–29.

Blake, S. & Ivey, G. N. 1986 Magma-mixing and the dynamics of withdrawal from stratified reservoirs. *J. Volcanol. Geoth. Res.* **27**, 153–178.

Craya, A. 1949 Recherches théoriques sur l'écoulement de couches superposées de fluides de densités différentes. *Huille Blanche* **4**, 44–55.

Freundt, A. & Tait, S. R. 1986 The entrainment of high-viscosity magma into low-viscosity magma in eruption conduits. *Bull. Volcanol.* **48**, 325–339.

Geller, A. S., Lee, S. H. & Leal, L. G. 1986 The creeping motion of a spherical particle normal to a deformable interface. *J. Fluid Mech.* **169**, 27–69.

HICKOX, C. E. 1971 Stability of two fluids in a pipe. *Phys. Fluids* **14**, 251–262.

HILDRETH, W. 1981 Gradients in silicic magma chambers: Implications for lithospheric magmatism. *J. Geophys. Res.* **86**, 10 153–10 192.

HUPPERT, H. E. & SPARKS, R. S. J. 1984 Double-diffusive convection due to crystallization in magmas. *Ann. Rev. Earth Planet. Sci.* **12**, 11–37.

IMBERGER, J. 1980 Selective withdrawal: a review. In *2nd Int. Symp. on Stratified Flows, Trondheim*, pp. 381–400. Tapir.

JANSONS, K. M. & LISTER, J. R. 1988 The general solution of Stokes flow in a half-space as an integral of the velocity on the boundary. *Phys. Fluids* (in press).

JOSEPH, D. D., RENARDY, M. & RENARDY, Y. 1984 Instability of the flow of two immiscible liquids with different viscosities in a pipe. *J. Fluid Mech.* **141**, 309–317.

KOYAGUCHI, T. 1985 Magma-mixing in a conduit. *J. Volcanol. Geoth. Res.* **25**, 365–369.

LADYZHENSKAYA, O. A. 1963 *The Mathematical Theory of Viscous Incompressible Flow*. Gordon & Breach.

LEE, S. H., CHADWICK, R. S. & LEAL, L. G. 1979 The motion of a sphere in the presence of a plane interface. *J. Fluid Mech.* **93**, 705–726.

LEE, S. H. & LEAL, L. G. 1982 The motion of a sphere in the presence of a deformable interface. II. A numerical study of the translation of a sphere normal to an interface. *J. Colloid. Interface Sci.* **87**, 81–106.

LORENTZ, H. A. 1907 A general theory concerning the motion of a viscous fluid. *Abhandl. Theoret. Phys.* **1**, 23.

MIKAMI, T., COX, R. G. & MASON, S. G. 1975 Breakup of extending liquid threads. *Int. J. Multiphase Flow* **2**, 113–138.

RALLISON, J. M. 1984 The deformation of small viscous drops and bubbles in shear flows. *Ann. Rev. Fluid Mech.* **16**, 45–66.

RALLISON, J. M. & ACRIVOS, A. 1978 A numerical study of the deformation and burst of a viscous drop in an extensional flow. *J. Fluid Mech.* **89**, 191–200.

SPARKS, R. S. J., HUPPERT, H. E. & TURNER, J. S. 1984 The fluid dynamics of evolving magma chambers. *Phil. Trans. R. Soc. Lond.* A **310**, 511–534.

SPERA, F. J. 1984 Some numerical experiments on the withdrawal of magma from crustal reservoirs. *J. Geophys. Res.* **89**, 8222–8236.

SPERA, F. J., YUEN, D. A., GREER, J. C. & SEWELL, G. 1986 Dynamics of magma withdrawal from stratified magma chambers. *Geology* **14**, 723–726.

TAYLOR, G. I. 1964 Conical free surfaces and fluid interfaces. In *Proc. 11th Intl Congr. Appl. Mech., Munich*, pp. 790–796. Springer.

TOMOTIKA, S. 1936 Breaking up of a drop of viscous fluid immersed in another viscous fluid which is extending at a uniform rate. *Proc. R. Soc. Lond.* A **153**, 302–318.

TUCK, E. O. & VANDEN-BROECK, J. M. 1984 A cusp-like free-surface flow due to a submerged source or sink. *J. Austral. Math. Soc.* B **25**, 443–450.

YOUNGREN, G. A. & ACRIVOS, A. 1975 Stokes flow past a particle of arbitrary shape: a numerical method of solution. *J. Fluid Mech.* **69**, 377–403.